Hierarchical Self-Assembly of Water-Soluble Fullerene Derivatives into Supramolecular Hydrogels

Rašović, Ilija; Piacenti, Alba R.; Contera, Sonia; Porfyrakis, Kyriakos

DOI:
10.1002/smll.202401963

RESEARCH ARTICLE

NANO · MICRO small
www.small-journal.com

Hierarchical Self-Assembly of Water-Soluble Fullerene Derivatives into Supramolecular Hydrogels

*Ilija Rašović, Alba R. Piacenti, Sonia Contera, and Kyriakos Porfyrakis**

Controlling the self-assembly of nanoparticle building blocks into macroscale soft matter structures is an open question and of fundamental importance to fields as diverse as nanomedicine and next-generation energy storage. Within the vast library of nanoparticles, the fullerenes—a family of quasi-spherical carbon allotropes—are not explored beyond the most common, C_{60}. Herein, a facile one-pot method is demonstrated for functionalizing fullerenes of different sizes (C_{60}, C_{70}, C_{84}, and $C_{90–92}$), yielding derivatives that self-assemble in aqueous solution into supramolecular hydrogels with distinct hierarchical structures. It is shown that the mechanical properties of these resultant structures vary drastically depending on the starting material. This work opens new avenues in the search for control of macroscale soft matter structures through tuning of nanoscale building blocks.

1. Introduction

Due to their high water content and similarities to the extracellular matrix of living tissues, hydrogels are emerging as key material to achieve transformative medical advances, in applications such as cellular scaffoldings in regenerative medicine/tissue engineering, tissue replacements, wound dressings, and drug/gene/protein/ribonucleic acid (RNA) delivery systems.[1,2] Much research aims to engineer both their chemical and mechanical properties to be able to facilitate the functional dynamics of healthy tissues while they are simultaneously able to deliver their therapeutic cargos such as cells or molecules. In this context, nanosized carbon structures such as graphene, carbon nanotubes, and fullerenes have unique chemical and physical properties that make them attractive for biomedical applications. They have been used in tissue engineering[3] biosensing and drug delivery.[4] Moreover, they have also shown antimicrobial activity.[5]

A key characteristic is that the surface of carbon nanomaterials can be functionalized to enhance their biocompatibility by increasing their water solubility.[6,7] Carbon nanomaterials can also be loaded with drugs for controlled local delivery applications[8] or used to enhance the electrical conductivity and mechanical stability of hydrogels for tissue engineering[9,10] as well as molecular transport properties.[11] It has been shown that the combination of carbon nanostructures and polymeric materials can result in supramolecular hydrogels with interesting properties such as self-healing.[12,13] Fullerenes are particularly useful because of their unique cage-like structure that can be used for functionalization or even encapsulation of molecules.[14] Fullerene cages are attractive candidates in medical applications including drug/gene delivery, cancer treatment, and diagnostics, and they have shown antiviral, antibacterial, and antioxidant activity.[15–19]

The physical properties of fullerenes make them ideal candidates to produce supramolecular structures and hydrogels without the need of an external polymeric matrix. While work has been done on fullerene "nanoarchitectonics"[20–23] and the creation of nanoscale supramolecular structures with C_{60} and its derivatives,[24–28] there are, to the best of our knowledge, no previous reports on supramolecular hydrogels manipulable by hand made solely from covalently-functionalized C_{60}. Further, again to the best of our knowledge, there have been no attempts made at incorporating higher fullerenes and their derivatives into such extended supramolecular structures.

Herein, we demonstrate the synthesis of new kinds of supramolecular hydrogel made from fullerenes of different sizes

I. Rašović
Department of Materials
University of Oxford
Parks Road, Oxford OX1 3PH, UK
I. Rašović
School of Metallurgy and Materials
University of Birmingham
Elms Road, Birmingham B15 2TT, UK
I. Rašović
EPSRC Centre for Doctoral Training in Topological Design
University of Birmingham
Birmingham B15 2TT, UK
A. R. Piacenti, S. Contera
Clarendon Laboratory
Department of Physics
University of Oxford
Parks Road, Oxford OX1 3PU, UK
K. Porfyrakis
Faculty of Engineering and Science
University of Greenwich
Central Avenue, Chatham Maritime, Kent ME4 4TB, UK
E-mail: K.Porfyrakis@greenwich.ac.uk

The ORCID identification number(s) for the author(s) of this article can be found under https://doi.org/10.1002/smll.202401963

DOI: 10.1002/smll.202401963

(C_{60}, C_{84}, and C_{90-92}) that have been hydroxylated and functionalized with hydrophilic oligoethylene glycol chains. Carrying out the reaction on fullerenes of different sizes, including C_{70}, allows us to interrogate the effect of fullerene shape on self-assembly behavior. We characterize the molecular building blocks with a suite of techniques and use AFM to characterize the elasticity of the hydrogels formed.

2. Results

Stable fullerene cages comprise pentagons and hexagons of covalently bonded carbon, with the isolated pentagon rule (IPR) giving rise to corannulene structures that induce strain and, therefore, sphericity.[29] The smallest and most abundant fullerene that obeys the IPR contains 60 carbon atoms (C_{60}) that form a truncated icosahedron with high I_h symmetry.[30] Its abundance and high symmetry (every carbon environment is identical) make its chemistry readily explorable.[31] The next most abundant fullerene, C_{70}, also exists as a single stable isomer, with D_{5h} symmetry; stable fullerenes with a higher number of carbon atoms exist as structural isomers with varied symmetries.[32] They are synthesized in very low yield and so their chemistry is vastly underexplored as compared to C_{60}.[29,31,33]

2.1. Functionalization of C_{60} Fullerene

In contrast to previous syntheses of C_{60} derivatives directly functionalized (TEGylated) with oligomeric ethylene glycol,[34,35] triethylene glycol monoethyl ether (TEG-MEE) was used—the terminal ethyl ether ensuring each oligomer chain could only covalently attach to one fullerene cage (see Experimental Section). A visible change in the color of the reaction solution, from purple to brown, could be seen within two minutes of adding NaOH. Initial evidence of a highly functionalized fullerene cage can be seen in the visible absorption spectrum of product **1** (Figure S1a, Supporting Information): it does not show the 425 nm shoulder diagnostic of a fullerene functionalized with few groups, instead displaying a featureless spectrum whose absorbance strongly increases toward the blue, indicative of a highly functionalized cage.[36] ^{1}H, ^{13}C, COSY, HSQC, and HMBC NMR (Figures S2–S5, Supporting Information) and FTIR spectra (Figures S7 and S8, Supporting Information) confirm the presence of TEG-MEE and its covalent attachment to the fullerene cage. ^{13}C NMR corroborates the evidence from the absorption spectrum that the cage is highly functionalized, due to the lack of peaks in the range 130–155 ppm (Figure S6, Supporting Information), which correspond to non-equivalent sp^2 carbons in functionalized C_{60} derivatives.[37] Instead, at least three unique carbon environments are observed downfield (δ 171.0, 164.8, and 163.21 ppm), indicative of oxidized carbons in the fullerene cage, such as carbonyl[38,39] and enol ether[40] groups, and carbons adjacent to those directly attached to hydroxyl groups.[41,42] FTIR confirms that hydroxylation of the fullerene cage has indeed occurred (Figure S8, Supporting Information).

A first attempt to quantify the number of TEG-MEE chains appended to the fullerene core was attempted using matrix-assisted laser desorption/ionization mass spectrometry (MALDI-TOF MS). Obtaining a mass spectrum of **1**, however, proved to be impossible. A summary of the matrices, matrix solution solvents, sample solution solvents, solution volume ratios, and laser powers attempted is given in Table S1 (Supporting Information). In light of no reliable MS data, elemental analysis (EA, see Table S2, Supporting Information) and thermal gravimetric analysis (TGA) were employed to estimate the average stoichiometric composition of **1**. The dynamic TGA trace of **1** shows four distinct mass losses (Figure S9, Supporting Information), in keeping with results seen for a tetraethylene glycol derivative synthesized using an analogous method.[34] The lack of any appreciable mass loss which correlates to the TEG-MEE control sample is good evidence that any chains present must be covalently linked to the fullerene cage.

Based on the mass losses in TGA and EA data, a series of simultaneous equations were numerically solved (see Supporting Information) to obtain an average stoichiometric composition for **1** of $C_{60}O_8(TEG)_5(OH)_{21}(O^-Na^+)_7{\cdot}5H_2O$ (TEG = TEG-MEE) with M_w 2453. The lowest energy structures for highly hydroxylated C_{60} derivatives are obtained when the functionalized carbons are on the same hexagon as each other, isolated from other such hydroxylated "islands".[43] Given this fact and the calculated average stoichiometric composition of **1**, its average structure was determined based on a repeatable functionalization motif (**Figure 1**).

2.2. Self-Assembly of Functionalized C_{60}

With a clearer picture of the molecular structure of **1** obtained, its behavior in aqueous solution could be interrogated. It has a high solubility in aqueous solution of 37 mg mL^{-1} at pH 7–8 (see Supporting Information). Its amphiphilic nature would suggest a propensity to aggregate in aqueous solution. Indeed, **1** was found to have a critical micelle concentration (CMC) of ≈1.0 mg mL^{-1} (Figure S1b, Supporting Information). Sessile drops of aqueous solution of **1** at a concentration (0.02 mg mL^{-1}) below the CMC were dropped onto glass microscope slides and left at room temperature to dry out before optical imaging. Chains and fractal patterns of spherical premicelles,[44–46] diameter ≈400 nm, formed (**Figure 2**) as the aqueous solvent front receded. The fractal nature of the 2D aggregation pattern is strong evidence of this process taking place in the diffusion-limited aggregation (DLA) regime.[47,48] Further, the calculated fractal dimension, $D_b = 1.83$, is characteristic of aggregates formed under DLA[49]; this behavior has previously been observed in the self-assembly of an alkyl-functionalized C_{60} derivative in THF:water solution[50] as well as in other self-assembling systems that lead to hierarchical structures based on functionalized peptides[51–53] and carbon nanotubes.[54]

In the DLA regime, every collision results in particles sticking together, thus implying that there are strong non-covalent interactions occurring between the constituent building blocks. It is unlikely that the short oligomeric TEG-MEE chains physically cross-link with each other to form self-assembled structures, as has been seen with star-shaped C_{60} derivatives functionalized with polyethylene glycol.[55] Molecular dynamics simulations have previously shown that the presence of up to six oligomeric ethylene glycol monomethyl ether (OEGMME) chains covalently grafted to C_{60} induces favorable non-covalent intermolecular interactions in water, leading to the formation of

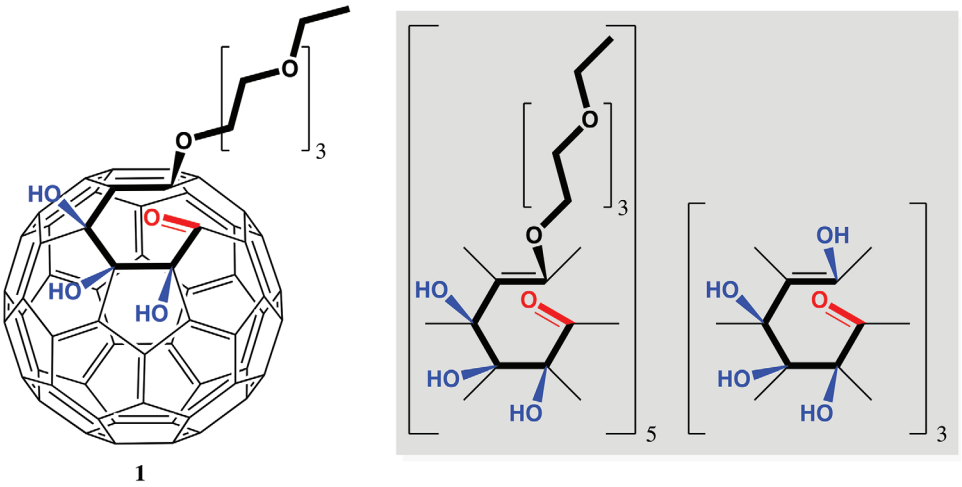

Figure 1. Average structure of TEGylated C_{60} **1**. Repeating the depicted functionalization motif of one hexagon eight times across the surface of the fullerene—in three of which the TEG-MEE chain is replaced by a hydroxyl group—gives the calculated average stoichiometry within one hydroxyl group. Calculated average structure contains 5 TEG-MEE chains, 28 hydroxyl groups (25% of these are in their saponified form, O^-Na^+), and 8 carbonyl groups. All wedge bonds radiate out from the fullerene surface.

linear chain-like aggregates.[56,57] These interactions were shown to act in three ways. First, the presence of covalently attached OEGMME chains induces a weak long-range (>12 Å) interaction between molecules, despite the chains' hydrophilicity. Second, the short-range (<12 Å) attraction between fullerenes in aqueous solution due to their hydrophobicity[58] is increased by the presence of covalently attached OEGMME—this is mediated by a favorable hugging interaction between OEGMME and the equator of an adjacent fullerene. Crucially, because the oligomeric chains are short, they do not sterically cover their own fullerenes to which they are attached, thus allowing this interaction between adjacent molecules to occur. Third, the even distribution of covalent attachment of OEGMME chains across the surface of C_{60} leads to anisotropic aggregation. Given the average stoichiometric composition of **1**, with five TEG-MEE chains per fullerene, it is reasonable to rationalize the experimentally observed aggregation behavior in terms of these computationally calculated non-covalent interactions. The presence of a high number of hydroxyl groups on the surface of the fullerene cage in **1** likely further strengthens this equatorial hugging interaction via hydrogen bonding between TEG-MEE chains and hydroxyl groups on adjacent fullerenes.

Solutions of **1** from 0.01 to 20 mg mL^{-1} were prepared and stored undisturbed in the dark (see Experimental Section). Within two weeks, solutions with concentration >0.5 mg mL^{-1} could be seen with the naked eye to contain floating gels, with a largest dimension in solution of 2 mm. Typically, only one such structure existed per solution. By six weeks, all gels had grown; the largest (from 2.0 mg mL^{-1} solution) with a largest dimension of 10 mm. Solutions with concentration <1.0 mg mL^{-1}

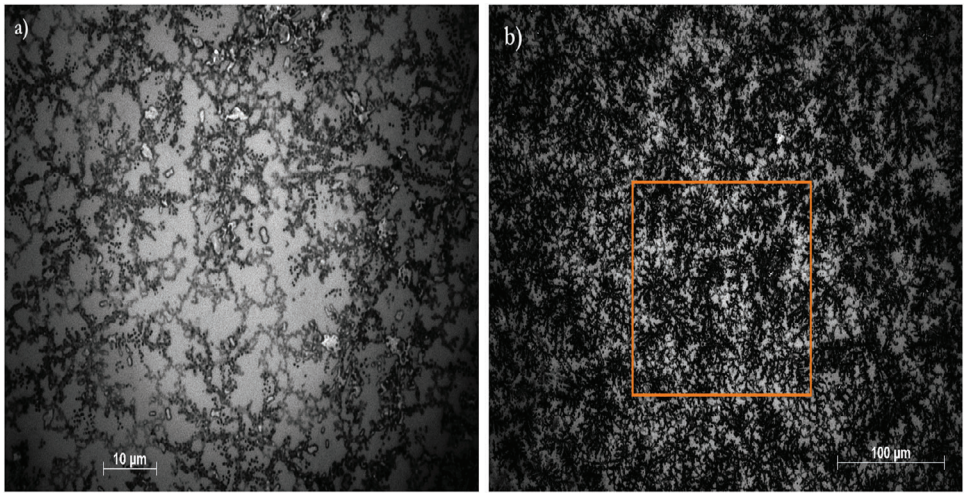

Figure 2. TEGylated C_{60} **1** forms premicelles. Transmission optical micrographs of a dried aqueous solution of TEGylated C_{60} **1** (0.02 mg mL^{-1}). Upon drying, the formation of a) chains and b) fractal patterns of spherical premicelles (diameter ≈400 and ≈1300 nm, respectively) can be seen. The fractal dimension of the highlighted area, D_b = 1.83, is indicative of the aggregation taking place in the diffusion-limited regime.

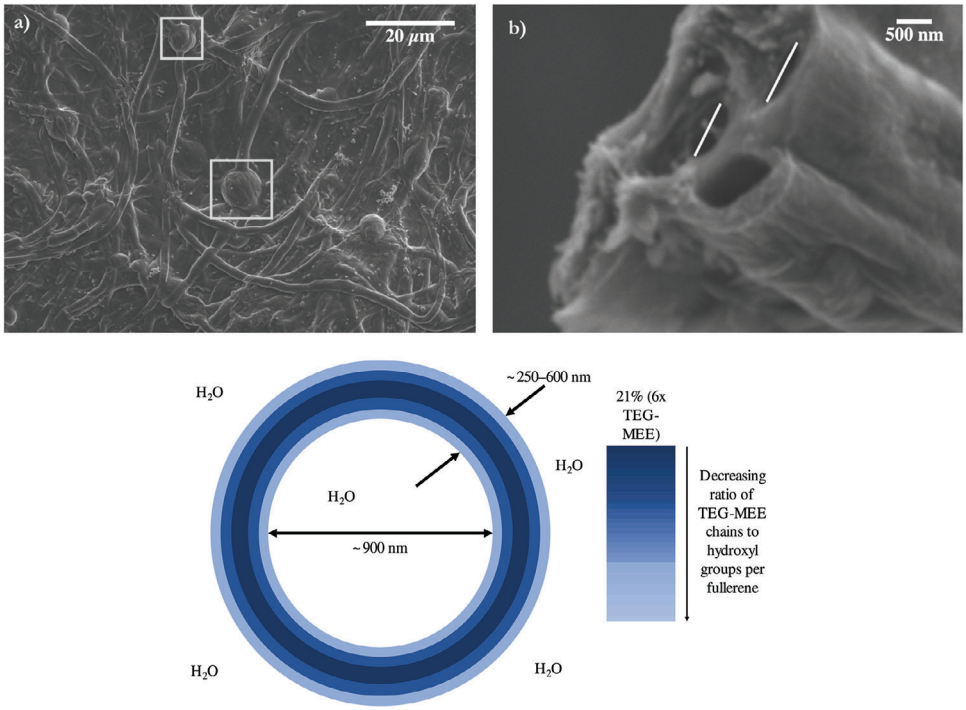

Figure 3. Hierarchical structure of supramolecular hydrogel formed by TEGylated C_{60} **1**. a) SEM micrograph of the flat xerogel formed when left to dry at room temperature. Although flattened in vacuo, spherical node junctions (5.6 and 8.3 μm in diameter) link a network of fibrillar strands (1.5–2 μm wide). Image acquired with 5 kV accelerating voltage, 30 pA probe current. b) By looking at the edge of the xerogel, the fibers are found to be hollow tubules of inner diameter ≈900 nm (calculated as the average of the two diameters highlighted). Image acquired with 5 kV accelerating voltage, 30 pA probe current. c) Proposed packing structure of **1** within a tubule. Those molecules with the highest number of TEG-MEE chains (up to 6, in accordance with previous computational studies) form the core of the tubular walls while the outermost molecules are those with a lower ratio of TEG-MEE chains to hydroxyl groups, increasing hydroxyl exposure to water.

still contained no aggregates visible to the naked eye. This correlates well with the observed CMC for **1** of 1.0 mg mL^{-1}. By six months, the largest gel (from 2.0 mg mL^{-1} solution) had a largest dimension in solution of 23 mm; solutions with concentration <1.0 mg mL^{-1} still contained no aggregates visible to the naked eye. This largest gel could be picked up and manipulated using tweezers without fracture, displaying viscoelastic behavior (see Video S1 and Figures S10 and S11, Supporting Information). No noticeable increase in size of any hydrogel was observed beyond six months. In contrast to the fast sub-CMC DLA regime, the slow rate of aggregation in solutions of concentration >1.0 mg mL^{-1} giving rise to large hydrogel structures is indicative of reaction-limited aggregation (RLA).[59] In this regime, not every collision between particles results in their sticking together. This situation arises above the CMC because the particles colliding are already formed into stable micellar structures. The long time taken for formation of hydrogel structures from **1** is in good agreement with previous experimental observations of self-assembly of C_{60} functionalized with polyethylene glycol.[60] As well as the kinetics of aggregation, the RLA regime is characterized by highly polydisperse solutions[59] evidence of which was seen by carrying out nanoparticle tracking analysis (Figure S12, Supporting Information). The supramolecular hydrogel[12,61–64] formed by **1** has a hierarchical structure (Figure 4a) comprised of a porous network (pore size 60 ± 15 μm) of hollow tubular fibers (inner diameter ≈900 nm, outer diameter 1.5–2 mm) connected by three-/four-arm junctions (**Figure 3a**). Such tubular structures can be rationalized by a graded internal packing: starting from molecules of **1** with six TEG-MEE chains attached at the core of the fiber wall, the ratio of TEG-MEE chains to hydroxyl groups per C_{60} decreases as the distance from the center of the wall increases (Figure 3c). In this way, TEG-MEE chains maximize their favorable non-covalent interaction with fullerenes— molecular dynamics simulations have shown that increasing the number of attached chains per fullerene beyond six leads to dispersion in solution rather than aggregation, as the chains can no longer wrap around neighboring cages[56]—whilst hydroxyl groups maximize their favorable hydrogen-bonding interaction with water.

2.3. Functionalization of Higher Fullerenes

Having observed the unprecedented formation of supramolecular hydrogels from near-spherical C_{60} by way of oligomer–fullerene non-covalent interactions, it was natural to interrogate this interaction further and see whether such hierarchical structures could be formed with larger (higher) fullerenes of different shapes: C_{70}, C_{84}, and a mixture of $C_{90–92}$. Like C_{60}, C_{70} has only one structural isomer but of a lower symmetry, D_{5h} (C_{60} has I_h symmetry). C_{84} has 24 structural isomers that obey the isolated pentagon rule (IPR)[32]; of these, the D_2 and D_{2d} isomers are the

most abundant and have the highest sphericity.[65] C_{90} has 46 structural isomers that obey the IPR,[32] 11 of which are kinetically and thermodynamically stable;[66] these are typically very low symmetry[67] with a highest symmetry point group of $C_{2v,}$[68] excluding the D_{5h} "nanotube" isomer that is synthesized via non-standard arc discharge conditions.[69] C_{92} has 86 IPR-compliant structural isomers, predominantly low symmetry.[32] $C_{90–92}$ are synthesized via arc discharge in such small quantities that differentiation and separation of the species by mass in HPLC is unfeasible; thus, given their collective low symmetry, they were collected and investigated as one fraction.

The TEGylation procedure as carried out for the synthesis of C_{60} derivative **1** was used on separate solutions of C_{70}, $C_{84,}$ and $C_{90–92}$ to yield derivatives **2**, **3**, and **4** respectively. As with C_{60}, a visible change in the color of the reaction solutions was observed within two minutes of adding NaOH. As with **1**, the visible absorption spectrum of TEGylated C_{70} **2** is featureless (Figure S13a, Supporting Information), indicative of a highly functionalized cage. ^{1}H, ^{13}C, COSY, HSQC, HMBC, and ^{13}C NMR (Figures S14–S18, Supporting Information) and FTIR spectra (Figure S19, Supporting Information) confirm the presence of TEG-MEE in **2**. As with **1**, FTIR confirms that hydroxylation of the fullerene cage has also occurred. Again, EA and TGA were employed to estimate the average stoichiometric composition of **2**. Unlike with **1**, dynamic TGA gave no compelling evidence for loss of covalently bound TEG-MEE chains (Figure S20, Supporting Information). This is perhaps unsurprising as it has previously been noted that addition of oxygen-containing groups to C_{70} occurs at slower rates than to C_{60} fullerene.[70] The average stoichiometric composition for **2** was calculated as $C_{70}O_{16}(OH)_9(O^-Na^+)_9{\cdot}4TEG{\cdot}18H_2O$ (TEG = TEG-MEE) with M_w 2668 (see Supporting Information). The lower ratio of polar functional groups to fullerene cage carbons (34:70 = 49%) compared to that for TEGylated C_{60} **1** (41:60 = 68%) corresponds well with the observed lower water solubility (1.04 mg mL^{-1}, see Supporting Information). ^{1}H and COSY NMR spectra of TEGylated C_{84} **3** (Figures S21 and S22, Supporting Information) confirmed the presence of TEG-MEE. The ready solubility of **3** and **4** in water (see Supporting Information) suggests the presence of hydroxyl and other oxygen-containing groups on the fullerene cages, as with **1** and **2**.

2.4. Self-Assembly of Functionalized Higher Fullerenes

As with C_{60} derivative **1**, TEGylated C_{70} **2** exhibits a CMC as evidenced by absorbance deviation[71,72] (Figure S18, Supporting Information). Amphiphiles with a greater proportion of hydrophobicity exhibit lower CMC values[73] so a CMC value of 0.05–0.1 mg mL^{-1} for **2** is consistent with the observation that **2** has a less functionalized cage than TEGylated C_{60} **1** (CMC 1.0 mg mL^{-1}) and is less soluble in water. Solutions of **2** from 0.02 to 1.0 mg mL^{-1} were prepared and stored undisturbed in the dark (see Experimental Section). Within two weeks, solutions with concentration >0.2 mg mL^{-1} had several small aggregates (<0.5 mm) visible to the naked eye, which had flocculated and sunk to the bottom of the vial; solutions with concentration <0.5 mg mL^{-1} showed no obvious aggregation. By six months, no change in the shape or size of the aggregates had occurred as judged by the naked eye, but the number of particles at the bottom of vials with solutions >0.2 mg mL^{-1} had increased. These were too small to pick up with tweezers and displayed none of the viscoelasticity of the TEGylated C_{60} hydrogel. These short-range structures comprised of small patchy flakes extending no more than 400 µm in two dimensions, with a thickness of only ≈110 nm (**Figure 4**b; Figure S23, Supporting Information). Unlike cycloadditions to the C_{70} cage, which attack the more strained polar α bonds[74] hydroxylation preferentially occurs across the equatorial belt.[70,75] Given the lack of compelling evidence for covalent attachment of TEG-MEE chains to C_{70}, it is reasonable to assume that hydroxylation (and introduction of other groups such as carbonyls) is the primary functionalization route of **2**, giving rise to a "reverse bola amphiphilic" structure[76] wherein a hydrophilic equator region is capped by two hydrophobic corannulene-like poles (Figure S23b, Supporting Information). The flat, flake-like morphology of aggregates of **2** can then be explained by extension of the concepts used to rationalize the self-assembly of **1**: the hugging interaction between TEG-MEE (this time non-covalently bound) and fullerene is favored around the equatorial region[56] and so, in the case of **2**, this leads to a patchwork-like aggregate morphology extending in two dimensions. The favorable hugging interaction between TEG-MEE and C_{70} is likely further strengthened by hydrogen bonding with surface hydroxyl groups.[77] The limited size of these structures can thus be rationalized, as the hydroxyl-filled equator of **2** is primarily involved in non-covalent interactions with TEG-MEE chains in the patchwork. Upon reaching a critical size limit, the aggregate does not have enough available hydrophilic groups to interact strongly with the surrounding water and it precipitates out of solution, as observed.

Solutions of TEGylated C_{84} **3** (3.3 mg mL^{-1}) and $C_{90–92}$ **4** (1.7 mg mL^{-1}) were prepared and stored undisturbed in the dark (see Experimental Section). Within two weeks, four very small black floating aggregates could be seen in solution of **3**, while a thin and wispy aggregate had started to form in solution of **4**. After six months, several black quasi-spherical aggregates (2–6 mm in solution) were floating in the solution of **3**—the biggest of these could be picked up with tweezers and displayed viscoelastic behavior like the hydrogel of TEGylated C_{60} **1**. Meanwhile, one large (21 mm in its largest dimension), white and wispy aggregate had formed in solution of **4**—it could also be picked up with tweezers and showed viscoelastic behavior. The self-assembled structures of both **3** (Figure 4c; Figure S24, Supporting Information) and **4** (Figure 4d; Figure S25, Supporting Information) closely resemble the hierarchical structure of that formed from TEGylated C_{60} **1**.

The aerogel of TEGylated C_{84} **3** comprises a dense interpenetrated network (average pore size 19 ± 5 µm) of hollow fibers (1–2 µm outer diameter, 0.6–0.9 µm inner diameter, 0.4–1.1 µm wall thickness). In places, the length of the fibers is stunted and flaky patches similar to those seen for C_{70} derivative **2** co-exist. C_{84} has 24 structural isomers that obey the IPR[32]; of these, the D_2 and D_{2d} isomers are the most abundant and have the highest sphericity.[65] Thus, it is expected that these two isomers are the primary components of **3**. Analogously to highly spherical C_{60} leading to the interpenetrated network of hollow fibers for **1**, the high sphericity of these major isomers plausibly explains the

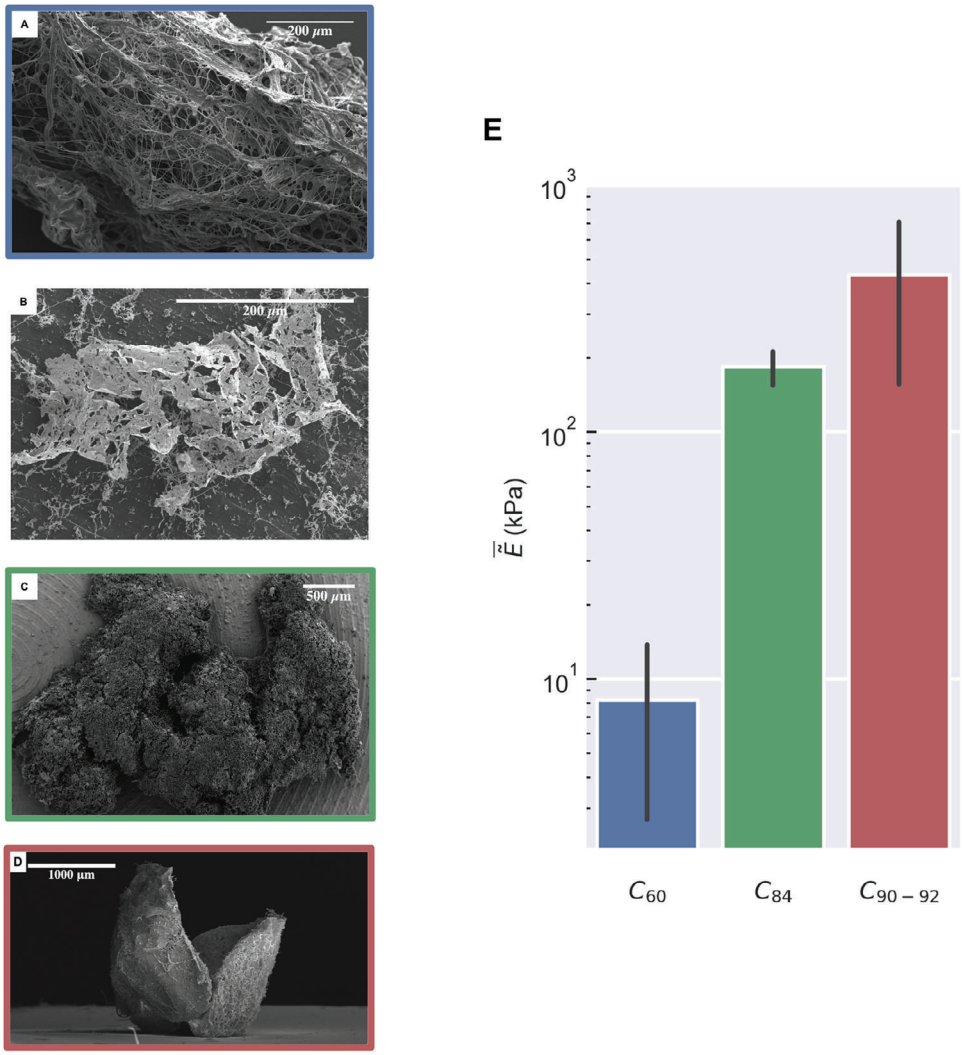

Figure 4. Hierarchical structures formed by TEGylated fullerenes of different sizes have different mechanical properties. a) SEM micrograph of aerogel of TEGylated C_{60} **1** after freeze-drying. The highly porous structure has an average pore size of 60 ± 15 μm, as determined by random sampling of 20 pores in ImageJ. Image acquired with 10 kV accelerating voltage, 100 pA probe current. b) SEM micrograph of an aggregated structure of TEGylated C_{70} **2** after freeze-drying. Image acquired with 10 kV accelerating voltage, 100 pA probe current. c) SEM micrograph of the aggregate of TEGylated C_{84} **3** (longest dimension 3.3 mm) shows it is more densely packed than the hydrogel for TEGylated C_{60} **1**. Image acquired with 10 kV accelerating voltage, 100 pA probe current. d) SEM micrograph showing the tulip-like structure of aggregate of TEGylated C_{90-92} **4** sitting on the SEM stub. After freeze-drying, the sample was a flat disc—upon prolonged exposure to the laboratory atmosphere, the disc slowly folded in on itself to this structure. Image acquired with 10 kV accelerating voltage, 100 pA probe current. e) Average reduced Young's moduli ($\bar{\tilde{E}}$) of hydrogels of TEGylated C_{60} (8.2 ± 6.2 kPa), C_{84} (183 ± 29 kPa) and C_{90-92} (432 ± 286 kPa), as determined by AFM-based nanoindentation. Error bars correspond to the standard deviation.

formation of the similar structure for **3**. Highly functionalized C_{84} derivatives have "ribbons" of unfunctionalized hexagons across their surface[78]—in the presence of multiple hydroxylation here, these ribbons likely form and provide appropriate sites for the hugging interaction between TEG-MEE and fullerene, enhanced by hydrogen bonding between TEG-MEE chains and surface hydroxyl groups. Other structural isomers whose functionalization patterns lead to hydrophobic corannulene-like regions across the cage—but not diametrically opposed—reasonably give rise to flat flaky regions (à la TEGylated C_{70} **2**).

The network of the aerogel of C_{90-92} **4** (average pore size 26 ± 11 μm, extending in two dimensions to ≈2 mm) is denser than for both C_{60} **1** and C_{84} **3**, with a global morphology intermediate of the fibrous networks of **1** and **3** and the flakes of C_{70} derivative **2** (Figure 4d; Figure S25, Supporting Information). The fibers have an outer diameter of ≈5 μm. C_{90} has 46 structural isomers that obey the IPR[32] 11 of which are kinetically and thermodynamically stable;[66] these are typically very low symmetry[67] with a highest symmetry point group of C_{2v},[68] excluding the D_{5h} "nanotube" isomer that is synthesized via non-standard arc discharge conditions.[69] C_{92} has 86 IPR-compliant structural isomers, predominantly low symmetry.[32] The positions of the most reactive sites on C_{90}[68] suggest that, under the TEGylation reaction conditions, hydrophobic corannulene-like regions exist across the cage but are not diametrically opposed (as with TEGylated C_{84} **3** but

in contrast to TEGylated C_{70} **2**). Thus, the dense interpenetrated structure of aerogel of C_{90-92} **4** is plausibly rationalized.

2.5. Mechanical Properties of Hydrogels

Atomic force microscopy (AFM) can be used to characterize the mechanical properties of hydrogels using nano-indentation (force measurement).[79] The Young's moduli of hydrogels of **1**, **3**, and **4** were measured in their hydrated state in an aqueous environment. Nanoindentation experiments were performed using a modified AFM cantilever with a micron-size bead attached. The self-assembled structures of C_{70} derivative **2** were too small to be isolated and too thin for this technique. The average reduced Young's modulus, $\overline{\tilde{E}}$, of C_{60} **1** hydrogel (8.2 ± 6.2 kPa) is two orders of magnitude less than that for both C_{84} **3** hydrogel (183 ± 29 kPa) and C_{90-92} **4** hydrogel (432 ± 286 kPa) (Figure 4e). The differences in $\overline{\tilde{E}}$ values can be rationalized based on the porosity of the hydrogel structures. C_{60} **1** hydrogel is the most porous and least dense—there is a small number of fibers behind each other to share the load from the AFM cantilever's bead. The large error arises from its irregular porosity. C_{84} hydrogel **3** is a denser network and so the load is transferred more easily to other fibers. Similarly, the presence of flat flaky regions increases the surface area of the sample—any applied load is thus spread over a larger surface area. The high density and regular porosity of this sample minimize the error in $\overline{\tilde{E}}$. C_{90-92} **4** hydrogel is the extreme example amongst these samples, with the flattest morphology of the interpenetrating networks. Thus, it has the highest $\overline{\tilde{E}}$. The large error arises because of differences in morphology across the sample's area.

3. Discussion

TEGylated C_{60} **1** can be thought of as an oligomeric star-shaped polymer[80] with an average of five arms radiating from its core. Similar fullerene-based systems functionalized with long-chain polystyrene[81] and polyethylene glycol[55,82] have been shown to form clusters >1 mm in diameter in aqueous solution, but there are few studies on oligoethylene glycol derivatives, despite their use in self-assembled monolayers[83] and self-assembled systems of other materials.[84–88] We appear to have supportive experimental evidence of an oligoethylene glycol–fullerene interaction that had previously only been studied computationally[56,57]—it is reasonably plausible that this "hugging" interaction is at least partly responsible for the formation of the observed extended supramolecular systems. The geometric and chemical complexity of fullerene derivatives **1**, **3**, and **4** renders calculation of a critical packing parameter, as per classical amphiphile self-assembly theory[73] impossible. The complex emergent structures of the supramolecular hydrogels appear to be bicontinuous phases[89] reminiscent of many structures found in nature.[90] The hollow fibers here for C_{60} **1** are larger than any fullerene-based supramolecular hierarchical structure before.[24,25] Porous materials such as this are highly sought after in the biomedical field for drug delivery purposes.[91] Furthermore, this is an example of a very porous material with a predominantly carbonaceous composition—such materials are particularly sought after for electrochemical applications such as next-generation capacitors.[92]

$\overline{\tilde{E}}$ of C_{60} **1** hydrogel is intermediate in the realm of biological tissues and is comparable to that of breast tumor, kidney, and lung tissue[93] and to that of carbon nanocomposite hydrogels for engineered cardiac tissue[9]; it is of average stiffness when compared with similar supramolecular hydrogels.[94] $\overline{\tilde{E}}$ of C_{84} **3** hydrogel and C_{90-92} **4** hydrogel can be classed as hard in the realm of biological tissues and are comparable to skeletal muscle and articular cartilage tissue.[93] Indeed, these are both an order of magnitude higher than for some "tough" polymeric supramolecular hydrogels whose mechanical properties deteriorate in the hydrated state.[95] Moreover, $\overline{\tilde{E}}$ of all the fullerene hydrogels studied herein falls in the elastic range of drug carriers used for drug delivery.[96] Supramolecular hydrogels incorporating carbon nanomaterials of different geometries and dimensionalities—1-D nanotubes, 2-D graphene oxide, and 3-D nanohorns—have previously shown differences in their morphologies and mechanical properties.[13] Until now though, such differences have not been explored between members of the same nanocarbon family.

A direct link between the fullerene building block and the reduced Young's modulus of its hydrogel resulting from functionalization with TEG-MEE can be inferred. However, given the differences in amount of non-covalently bound TEG-MEE for the higher fullerene samples, one should proceed with caution. Qualitatively, a reasonable relationship between fullerene building block (and the likelihood of the presence of corannulene-like hydrophobic regions post-functionalization) and presence of flat flake-like morphologies can be made. It is encouraging to note that the strongest of these fullerene hydrogels fares very well against supramolecular polymer opposition. These fullerene hydrogels, thanks to their porous structure, water content, and elastic properties similar to those of biological tissues and drug carriers, are viable candidates for biomedical applications. The measured pore sizes and fiber diameters are both of the right orders of magnitude to make these materials viable for cell scaffolds.[97] The use of fullerenes as the base material provides a proof-of-concept platform for incorporating endohedral fullerenes for additional functionality and raises the question of what self-assembled structures, with what functionality, could be made if other functional fullerene derivatives were further functionalized using this method.

The molecule–aggregate structure relations for each of the TEGylated fullerene derivatives synthesized and their corresponding self-assembled structures are summarized in **Table 1**. Given the lack of covalent grafting of TEG-MEE to C_{70} cages and assumed lesser reactivity of C_{84} and C_{90-92}, these two higher fullerenes were expected to be hydroxylated in part but only non-covalently associated with TEG-MEE. Given the observed morphologies, a relationship between fullerene shape and self-assembled structure after this functionalization protocol is proposed: the area of flat flake-like morphologies increases with the likelihood of opposed corannulene-like hydrophobic regions existing in the fullerene building block after functionalization. As Table 1 demonstrates, C_{60} derivative **1** and C_{70} derivative **2** are the two extreme cases, with C_{84} derivative **3** and C_{90-92} derivative **4** intermediate of the two. The proposed link between molecular fullerene building block and hydrogel structure suggests an

Table 1. Molecule structure–hydrogel structure–stiffness relations for TEGylated fullerene derivatives of different sizes.

Fullerene [sample]	Oxidized coverage of fullerene[a)]	Corannulene-like regions after functionalization?	TEG-MEE Covalently bound?	Hydrogel size [Largest dimension]	Hydrogel morphology	Average pore size [μm]	Fiber diameter [μm]	Reduced Young's modulus, $\overline{E}$ [kPa]
C_{60} (1)	60%, evenly distributed	No	Yes	Large, 23 mm	Porous with hollow fibers	60 ± 15	1.5–2	8.2 ± 6.2
C_{70} (2)	49%, around the equator	Yes, diametrically opposed	No	Small, 400 μm	No hydrogel, flat flakes	N/A	N/A	N/A
C_{84} (3)	Unknown, likely presence of hydrophobic ribbons	Yes, not diametrically opposed	Unlikely	Medium, 2 mm	Porous with hollow fibers, regions of flakes	19 ± 5	1–2	183 ± 29
$C_{90–92}$ (4)	Unknown, likely isolated hydrophilic islands	Yes, not diametrically opposed	Unlikely	Medium, 2 mm	Porous, some flat regions	26 ± 11	4–5	432 ± 286

[a)] Ratio of functionalized to non-functionalized carbons in the fullerene cage.

ability to tune the final properties of a desired supramolecular entity based on its starting material. Aside from this, a more general conclusion can be drawn that hydroxylation of fullerene cages of different sizes in the presence of TEG-MEE leads to extended hierarchical supramolecular architectures. Most excitingly, this has been shown to be applicable to higher fullerenes C_{84} and $C_{90–92}$, providing the first example of a route to synthesizing macroscopic materials with potential medical utility from these rare building blocks.

The self-assembled fullerene structures synthesized here add to a body of supramolecular systems based on synthetic amphiphiles in an emerging field that includes, for example, peptide amphiphiles.[98,99] Further comparative investigation of the differences and similarities of these systems is warranted as we strive to gain a better understanding of how we can move rationally from the nano to the macro.[100]

4. Experimental Section

Materials: All commercial solvents, reactants, and reagents were purchased from Sigma-Aldrich (United Kingdom) and used as purchased unless otherwise stated. Fullerenes C_{60} (99+% purity) and C_{70} (95+% purity) were used as purchased from Materials and Electrochemical Research (MER) Corporation (Arizona, USA). Fullerenes C_{84} and $C_{90–92}$ were produced using a standard in-house procedure (see below). Grade 2 deionized water adhering to ISO3696 purchased from Chemiphase (United Kingdom) was used unless otherwise stated.

Molecular Characterisation: ^{1}H, ^{13}C, COSY, HSQC, and HMBC NMR spectra were recorded using Bruker AVIII400 and Bruker AVIII500 (with He cryoprobe) spectrometers. Mass spectra were recorded on a Bruker Microflex LT matrix-assisted laser desorption/ionization time-of-flight mass spectrometer (MALDI-TOF MS). FTIR spectra were recorded at room temperature on a Varian Excalibur FTS 3500 FT-IR with golden gate diamond attenuated total reflection (ATR). Steady-state UV-vis absorption spectra were recorded in H_2O at 298 K on a dual-beam JASCO V-570 spectrophotometer (scan rate 200 nm min^{-1}), with reference to a solvent blank; quartz cuvettes with 1 cm path length were used in all cases. Dynamic TGA measurements were carried out on a Perkin Elmer Pyris 1 under nitrogen atmosphere (200 mL min^{-1}), at a constant rate of change of temperature of 10 °C min^{-1} in the range 40 to 1200/1400 °C, collecting data points every 0.2 s; samples (at least 2 mg) were loaded in ceramic TGA pans (Perkin Elmer, United Kingdom) and calibrated against an empty pan. All elemental analysis measurements were carried out by MEDAC Ltd. (Surrey, United Kingdom).

Higher Fullerene Synthesis: Standard Krätschmer-Huffman arc discharge[101] was employed. Rods (10 × 10 × 100 mm) of pure graphite or Gd-doped (2 wt% Gd_2O_3) graphite were purchased from Toyo Tanso (Osaka, Japan) and used as electrodes—the anode-cathode distance was <1 cm. Optimal conditions for fullerene production were set: the water-cooled arc discharge chamber was evacuated (10^{-4} Torr) before being filled with He gas (50 mbar), and a 200 A direct current was used for the arc.[102] Being careful not to exceed the maximum operating temperature (≈3700 °C) for more than ten seconds at a time, the rods were burnt down. The resulting soot was collected from the chamber and dissolved in toluene. This solution then underwent Soxhlet extraction typically for 48 h in order to extract soluble empty-cage fullerenes from other insoluble carbonaceous material. Reverse-phase HPLC (Japan Analytical Industry (JAI) LC-9103 Preparative HPLC with a modular Hitachi L-7150 pump and JAI UV Detector 3702 at 312 nm absorption) with a Cosmosil Buckyprep-M column (20.0 mm ID x 250 mm, toluene, 16 mL min^{-1} flow rate) was then used on this concentrated solution to isolate the different sized cages. Structural isomers of the same sized cages with different symmetries were not separated from each other.[103]

Fullerene Functionalization: Compound **1**: To C_{60} (40 mg, 55.6 mmol, 1 eq) dissolved in toluene (25 mL) was added triethylene glycol monoethyl ether (5 mL, 28.6 mmol, 515 eq) and NaOH (217 mg, 5.4 mmol, 97 eq). The stoppered reaction proceeded for 21 h at room temperature. A volumetric excess of EtOAc (75 mL) was added to the reaction flask, which was then placed in the fridge (2 °C) overnight, giving a brown precipitate. The contents of the flask were filtered (PTFE, 0.2 μm), leaving a brown precipitate on the filter and a cloudy yellow filtrate. The process was repeated with 150 mL EtOAc on the cloudy filtrate, giving a brown precipitate on the filter and a clear pale yellow filtrate. The brown precipitates were redispersed in EtOH (35 mL) with reasonable solubility before EtOAc (70 mL) was again added and the solution was left in the fridge (2 °C) overnight, giving a brown precipitate. This EtOH redispersion–EtOAc precipitation–filtration process was repeated once again, and the resulting precipitate dried *in vacuo* to give **1** as a brown powder (121 mg). ^{1}H NMR (500 MHz, D_2O) δ 3.67–3.54 (12H, m, CH_2), 3.51 (2H, q, J = 7.1 Hz, CH_2), 1.10 (3H, t, J = 7.1 Hz, CH_3). ^{13}C NMR (126 MHz, D_2O) δ 171.03, 164.84, 163.24, 163.19, 71.61, 69.54, 69.52, 69.37, 68.83, 68.35, 66.56, 63.78, 60.25, 13.97. FTIR (cm^{-1}) 3407*m*, 3284*m*, 3169*m*, 3003*w*, 2984*w*, 2936*w*, 1565*s*, 1404*s*, 1118*m*, 1044*m*, 1016*m*, 924*w*, 870*w*, 646*m*, 620*m*.

Compound **2**: To C_{70} (30 mg, 41.7 mmol, 1 eq) dissolved in toluene (18 mL) was added triethylene glycol monoethyl ether (3.75 mL, 21.4 mmol, 515 eq) and NaOH (192 mg, 4.80 mmol, 115 eq). The stoppered reaction proceeded for 21 h at room temperature. A volumetric excess of EtOAc (55 mL) was added to the reaction flask, which was then

placed in the fridge (2 °C) overnight, giving a brown precipitate. The contents of the flask were filtered (PTFE, 0.2 µm), leaving a dark grey precipitate on the filter and a very dilute yellow filtrate. The dark grey precipitate was rinsed with EtOH (30 mL), giving a brown filtrate and leaving a brown precipitate on the filter paper. This precipitate was dried *in vacuo* to give **2** as a brown powder (98 mg). ^{1}H NMR (500 MHz, D_2O) δ 3.69–3.53 (12H, m, CH_2), 3.50 (2H, q, J = 7.0 Hz, CH_2), 1.10 (3H, t, J = 7.1 Hz, CH_3). ^{13}C NMR (126 MHz, D_2O) δ 171.08, 166.31, 71.66, 69.58, 69.56, 69.43, 66.60, 60.31, 14.02. FTIR (cm^{-1}) 3449*m*, 3273*m*, 3055*m*, 1645*m*, 1429*s*, 1410*s*, 1105*m*, 1058*m*, 1006*m*, 874*m*, 847*m*, 615*s*, 604*s* cm^{-1}.

Compound **3**: To C_{84} (5 mg, 4.96 mmol, 1 eq) dissolved in toluene (8 mL) was added triethylene glycol monoethyl ether (1 mL, 5.72 mmol, 1154 eq) and NaOH (68 mg, 1.70 mmol, 343 eq). The stoppered reaction proceeded for 21 h at room temperature. A volumetric excess of EtOAc (25 mL) was added to the reaction flask, which was then placed in the fridge (2 °C) overnight, giving a light brown precipitate. The contents of the flask were filtered (PTFE, 0.2 µm), leaving a dark grey precipitate on the filter and a dilute yellow filtrate. The dark grey precipitate was rinsed with acetone (20 mL), giving a very pale yellow filtrate and leaving a light brown precipitate on the filter paper. This precipitate was dried *in vacuo* to give **3** as a brown powder (23 mg). ^{1}H NMR (400 MHz, D_2O) δ 3.68–3.55 (12H, m, CH_2), 3.52 (2H, q, J = 7.0 Hz, CH_2), 1.11 (3H, t, J = 7.1 Hz, CH_3).

Compound **4**: To a mixture of C_{90-92} (2 mg, 1.85 mmol, 1 eq) dissolved in toluene (4 mL) was added triethylene glycol monoethyl ether (0.7 mL, 4.01 mmol, 2165 eq) and NaOH (52 mg, 1.30 mmol, 703 eq). The stoppered reaction proceeded for 21 h at room temperature. A volumetric excess of EtOAc (15 mL) was added to the reaction flask, which was then placed in the fridge (2 °C) overnight, giving a light brown precipitate. The contents of the flask were filtered (PTFE, 0.2 µm), leaving a light grey precipitate on the filter and a dilute yellow filtrate. This light grey precipitate was dried *in vacuo* to give **4** as a brown powder (12 mg).

Hydrogel Synthesis: Serial dilutions of functionalized C_{60}, **1** (20, 10, 5.0, 2.0, 1.0, 0.5, 0.2, 0.1, 0.05, 0.02, and 0.01 mg mL^{-1}) and functionalized C_{70}, **2** (1.0, 0.5, 0.2, 0.1, 0.05, and 0.02 mg mL^{-1}) were prepared in aqueous solution. 2 mL of each sample were pipetted into 20 mL glass vials, the lids screwed on and sealed with Parafilm M, and the vials stored undisturbed in a dark cupboard for up to six months. Aqueous solutions of functionalized C_{84}, **3** (3.3 mg mL^{-1}) and functionalized C_{90-92}, **4** (1.7 mg mL^{-1}) were prepared and pipetted into 20 mL glass vials, the lids screwed on and sealed with Parafilm M, and the vials stored undisturbed in a dark cupboard for up to six months.

Nanoparticle Tracking Analysis: Nanoparticle tracking analysis was carried out on a Malvern Panalytical Nanosight LM10 at room temperature (638 nm laser); eight measurement runs were conducted per sample.

Optical Microscopy: Samples were pipetted onto glass microscope slides and imaged in transmission mode on a Motic BA210 binocular optical microscope. Images were analyzed using ImageJ software. Fractal dimensions were calculated using the FracLac plugin for this software: the image was converted to a binary image, a maximum of 12 grid positions was selected, and box sizes were selected using the default sampling size, with the minimum box size unspecified and the maximum at 45% of the sampled area.

Scanning Electron Microscopy: Samples were pipetted or, if large enough, placed with tweezers onto an SEM stub and then frozen for 24 h at –20 °C before being freeze-dried for 24 h at 0 °C and 0.05 atm, as per procedure for collagen tissue scaffolds.[104,105] The freeze-dried samples were then placed on another SEM stub covered with double-sided conductive copper tape before being coated with 5–10 nm of gold by a Bio-Rad E5000 sputter coater. Secondary electron images were acquired on a Zeiss EVO MA10 with an accelerating voltage of 5–10 kV and a probe current of 30–100 pA. Images were analyzed using ImageJ software.

Atomic Force Microscopy Force Measurements: Force indentation measurements on all samples were performed at room temperature with an MFP-3D AFM (Asylum Research, Oxford Instruments, Santa Barbara, CA). AC240 cantilevers (Olympus, Japan) with nominal spring constant 2 Nm^{-1} and resonance frequency 70 kHz were used with an attached colloidal polystyrene bead of diameter 20 ± 0.3 mm (Sigma Aldrich).[106] The optical lever sensitivity of the cantilever was determined by indenting a hard substrate, followed by the calculation of the spring constant using the thermal noise method.[107] Force measurements were performed with a maximum loading force of 70 nN at high speed (40 µm s^{-1}) to reduce the time-dependent behavior of the hydrogels.[106,108] Samples were glued (with either medical adhesive (Hollister) or epoxy (Double Bubble Loctite)) on top of double-sided tape and stuck to plastic containers. After the glue dried, samples were immersed in ultrapure (Milli-Q) water. At least five positions were indented per sample; 100 force curves were recorded at each position. Data were acquired using the Oxford Instruments Asylum Research software based on Igor Pro. Data analysis was performed using a Python code developed in-house. The contact point for each force indentation curve was obtained using the FIV method.[106] The mechanical properties were quantified by fitting the approach curves with the Hertz model.[109,110] By neglecting the deformation of the much stiffer AFM tip, the reduced Young's modulus of the sample can be defined as $\tilde{E} = E/(1-\nu^2)$, where E and ν are the Young's modulus and the Poisson's ratio of the sample.[111] Since ν of the fullerene hydrogels is unknown, results are reported with $\tilde{E}$. $\tilde{E}$ calculated for each indentation curve was averaged over the 100 indentation curves for each tested position on the sample and averaged over all the measured positions across each sample ($\bar{\tilde{E}}$).

Supporting Information

Supporting Information is available from the Wiley Online Library or from the author.

Acknowledgements

I.R. and K.P. thank EPSRC for funding [EP/K030108/1]. The authors thank Dr. Panagiotis Dallas, Georgios Velkos, and Michelle Van for their contributions in synthesizing the higher fullerenes. The authors also thank Prof. Jan Czernuszka and his group members, Fang Li and Sonia Iftekhar, for help with freeze-drying, and Jennifer Holter at the David Cockayne Centre for Electron Microscopy for capturing SEM images. The authors thank the National Mass Spectrometry Facility at Swansea University for analyzing several samples. ARP thanks EPSRC, the Sidney Perry Foundation, the Blanceflor Foundation, the Borsa di Perfezionamento all'Estero of Sapienza University of Rome, and Fondazione Angelo Della Riccia. The authors also thank Dr Andrea Bonilla-Brunner and Dr Jacob Kienast (Seifert) for their help with AFM.

Conflict of Interest

The authors declare no conflict of interest.

Author Contributions

I.R. carried out the synthesis and characterization. A.R.P. carried out the AFM. All authors contributed to writing and editing the manuscript.

Data Availability Statement

The data that support the findings of this study are available in the supplementary material of this article.

Keywords

hydrogels, self-assembly, supramolecular structures, water-soluble fullerenes

Received: March 12, 2024
Revised: May 20, 2024
Published online:

[1] M. P. Lutolf, J. A. Hubbell, *Nat. Biotechnol.* **2005**, *23*, 47.
[2] G. Sun, X. Zhang, Y.-I. Shen, R. Sebastian, L. E. Dickinson, K. Fox-Talbot, M. Reinblatt, C. Steenbergen, J. W. Harmon, S. Gerecht, *Proc. Natl. Acad. Sci. USA* **2011**, *108*, 20976.
[3] R. Eivazzadeh-Keihan, A. Maleki, M. de la Guardia, M. S. Bani, K. K. Chenab, P. Pashazadeh-Panahi, B. Baradaran, A. Mokhtarzadeh, M. R. Hamblin, *J. Adv. Res.* **2019**, *18*, 185.
[4] H. Wang, Q. Chen, S. Zhou, *Chem. Soc. Rev.* **2018**, *47*, 4198.
[5] A. Al-Jumaili, S. Alancherry, K. Bazaka, M. V. Jacob, *Materials* **2017**, *10*, 1066.
[6] W. Liu, G. Speranza, *J. Carbon Res.* **2019**, *5*, 72.
[7] N. M. Bardhan, *J. Mater. Res.* **2017**, *32*, 107.
[8] R. G. Mendes, A. Bachmatiuk, B. Büchner, G. Cuniberti, M. H. Rümmeli, *J. Mater. Chem. B* **2013**, *1*, 401.
[9] S. R. Shin, S. M. Jung, M. Zalabany, K. Kim, P. Zorlutuna, S. B. Kim, M. Nikkhah, M. Khabiry, M. Azize, J. Kong, K.-T. Wan, T. Palacios, M. R. Dokmeci, H. Bae, X. (S.). Tang, A. Khademhosseini, *ACS Nano* **2013**, *7*, 2369.
[10] S. Marchesan, L. Ballerini, M. Prato, *Science* **2017**, *356*, 1010.
[11] E. Axpe, L. Bugnicourt, D. Merida, M. Goiriena-Goikoetxea, I. Unzueta, R. Sanchez-Eugenia, J. A. Garcia, F. Plazaola, S. Contera, *J. Mater. Chem. B* **2015**, *3*, 3169.
[12] R. Dong, Y. Pang, Y. Su, X. Zhu, *Biomater. Sci.* **2015**, *3*, 937.
[13] D. Iglesias, M. Melle-Franco, M. Kurbasic, M. Melchionna, M. Abrami, M. Grassi, M. Prato, S. Marchesan, *ACS Nano* **2018**, *12*, 5530.
[14] A. Popov, S. Yang, L. E. F Dunsch, *Chem. Rev.* **2013**, *113*, 5989.
[15] A. Montellano, T. Da Ros, A. Bianco, M. Prato, *Nanoscale* **2011**, *3*, 4035.
[16] R. Partha, J. L. Conyers, *Int. J. Nanomed.* **2009**, *4*, 261.
[17] I. Rašović, *Mater. Sci. Technol.* **2017**, *33*, 777.
[18] E. Castro, A. H. Garcia, G. Zavala, L. Echegoyen, *J. Mater. Chem. B* **2017**, *5*, 6523.
[19] S. Goodarzi, T. Da Ros, J. Conde, F. Sefat, M. Mozafari, *Mater. Today* **2017**, *20*, 460.
[20] L. K. Shrestha, Q. Ji, T. Mori, K. Miyazawa, Y. Yamauchi, J. P. Hill, K. Ariga, *Chem. – An Asian J.* **2013**, *8*, 1662.
[21] M. Ramanathan, L. K. Shrestha, T. Mori, Q. Ji, J. P. Hill, K. Ariga, *Phys. Chem. Chem. Phys.* **2013**, *15*, 10580.
[22] X. Shen, J. Song, K. Kawakami, K. Ariga, *Materials* **2022**, *15*, 5404.
[23] K. Minami, J. Song, L. K. Shrestha, K. Ariga, *Appl. Mater. Today* **2021**, *23*, 100989 .
[24] T. Haino, Y. Matsumoto, Y. Fukazawa, *J. Am. Chem. Soc.* **2005**, *127*, 8936.
[25] M. Sathish, K. Miyazawa, T. Sasaki, *Chem. Mater.* **2007**, *19*, 2398.
[26] O. Gavat, T. M. Nguyet Trinh, E. Moulin, T. Ellis, M. Maaloum, E. Buhler, G. Fleith, J.-F. Nierengarten, N. Giuseppone, *Chem. Commun.* **2018**, *54*, 7657.
[27] R. Partha, M. Lackey, A. Hirsch, S. W. Casscells, J. L. Conyers, *J. Nanobiotechnol.* **2007**, *5*, 6.
[28] F. Lu, E. A. Neal, T. Nakanishi, *Acc. Chem. Res.* **2019**, *52*, 1834.
[29] F. Diederich, R. L. Whetten, *Acc. Chem. Res.* **1992**, *25*, 119.
[30] H. W. Kroto, J. R. Heath, S. C. O'Brien, R. F. Curl, R. E. Smalley, *Nature* **1985**, *318*, 162.
[31] A. Hirsch, M. Brettreich, F. Wudl, *Fullerenes: Chemistry and Reactions*, John Wiley & Sons, Hoboken, New Jersey, U.S. **2006**.
[32] P. W. Fowler, D. E. Manolopoulos, *An Atlas of Fullerenes*, Dover Publications, Mineola, New York **2006**.
[33] S. I. Troyanov, S. Yang, C. Chen, E. Kemnitz, *Chem. – A Eur. J.* **2011**, *17*, 10662.
[34] J. Jeong, J. Jung, M. Choi, J. W. Kim, S. J. Chung, S. Lim, H. Lee, B. H. Chung, *Adv. Mater.* **2012**, *24*, 1999.
[35] A. S. Stasheuski, V. A. Galievsky, A. P. Stupak, B. M. Dzhagarov, M. J. Choi, B. H. Chung, J. Y. Jeong, *Photochem. Photobiol.* **2014**, *90*, 997.
[36] A. Hirsch, M. Brettreich, *Fullerenes: Chemistry and Reactions*, John Wiley & Sons, Hoboken, New Jersey, U.S. **2005**.
[37] A. R. Tulyabaev, I. I. Kiryanov, I. S. Samigullin, L. M. Khalilov, *Int. J. Quantum Chem.* **2017**, *117*, 7.
[38] A. Arrais, E. Diana, *Fullerenes, Nanotub. Carbon Nanostruct.* **2003**, *11*, 35.
[39] Z. Wang, Z. Lu, Y. Zhao, X. Gao, *Nanoscale* **2015**, *7*, 2914.
[40] L. Y. Chiang, J. W. Swirczewski, C. S. Hsu, S. K. Chowdhury, S. Cameron, K. Creegan, *J. Chem. Soc. Chem. Commun.* **1992**, 1791.
[41] E. E. Fileti, R. Rivelino, *Chem. Phys. Lett.* **2009**, *467*, 339.
[42] H. He, L. Zheng, P. Jin, M. Yang, *Comput. Theor. Chem.* **2011**, *974*, 16.
[43] R. A. Guirado-López, M. E. Rincón, *J. Chem. Phys.* **2006**, *125*, 154312.
[44] R. Hadgiivanova, H. Diamant, *J. Chem. Phys.* **2009**, *130*, 114901.
[45] X. Cui, S. Mao, M. Liu, H. Yuan, Y. Du, *Langmuir* **2008**, *24*, 10771.
[46] H. Zhong, L. Yang, X. Yang, G. Zeng, Z. Liu, Y. Liu, X. Yuan, *RSC Adv.* **2015**, *5*, 88578.
[47] P. Meakin, *Adv. Colloid Interface Sci.* **1987**, *28*, 249.
[48] R. Jullien, *Contemp. Phys.* **1987**, *28*, 477.
[49] M. Y. Lin, H. M. Lindsay, D. A. Weitz, R. Klein, R. C. Ball, P. Meakin, *J. Phys. Condens. Matter* **1990**, *2*, 3093.
[50] S. S. Gayathri, A. Patnaik, *J. Chem. Phys.* **2006**, *124*, 131104.
[51] Z. Gu, G. Patterson, R. Cao, B. Armitage, *J. Polym. Sci. Part B Polym. Phys.* **2003**, *41*, 3037.
[52] W. Wang, Y. Chau, *Soft Matter* **2009**, *5*, 4893.
[53] E. Mayans, G. Ballano, J. Casanovas, L. J. del Valle, M. M. Pérez-Madrigal, F. Estrany, A. I. Jiménez, J. Puiggalí, C. Cativiela, C. Alemán, *Soft Matter* **2016**, *12*, 5475.
[54] Z. Liu, X. Kong, *Phys. Chem. Chem. Phys.* **2010**, *12*, 9475.
[55] V. T. Lebedev, D. N. Orlova, E. Y. Melenevskaya, V. V. Shamanin, L. V. Vinogradova, *Russ. J. Appl. Chem.* **2011**, *84*, 278.
[56] D. Bedrov, G. D. Smith, L. Li, *Langmuir* **2005**, *21*, 5251.
[57] J. B. Hooper, D. Bedrov, G. D. Smith, *Langmuir* **2008**, *24*, 4550.
[58] J. Brant, H. Lecoanet, M. R. Wiesner, *J. Nanoparticle Res.* **2005**, *7*, 545.
[59] M. Y. Lin, H. M. Lindsay, D. A. Weitz, R. C. Ball, R. Klein, P. Meakin, *Phys. Rev. A* **1990**, *41*, 2005.
[60] N. Manolova, I. Rashkov, F. Beguin, H. Van Damme, *J. Chem. Soc. Chem. Commun.* **1993**, 1725.
[61] D. Wen, A. Eychmüller, *Chem. Commun.* **2017**, *53*, 12608.
[62] X. Yan, S. Li, T. R. Cook, X. Ji, Y. Yao, J. B. Pollock, Y. Shi, G. Yu, J. Li, F. Huang, P. J. Stang, *J. Am. Chem. Soc.* **2013**, *135*, 14036.
[63] H. Wang, Q. Chen, S. Zhou, *Chem. Soc. Rev.* **2018**, *47*, 4198.
[64] C.-W. Chu, B. J. Ravoo, *Chem. Commun.* **2017**, *53*, 12450.
[65] D. S. Sabirov, O. Ori, I. László, *Fullerenes, Nanotub. Carbon Nanostruct.* **2018**, *26*, 100.
[66] M. Watanabe, D. Ishimaru, N. Mizorogi, M. Kiuchi, J. I. Aihara, *J. Mol. Struct. THEOCHEM* **2005**, *726*, 11.
[67] H. Yang, B. Q. Mercado, H. Jin, Z. Wang, A. Jiang, Z. Liu, C. M. Beavers, M. M. Olmstead, A. L. Balch, *Chem. Commun.* **2011**, *47*, 2068.
[68] R. L. Murry, G. E. Scuseria, *J. Phys. Chem.* **1994**, *98*, 4212.
[69] H. Yang, C. M. Beavers, Z. Wang, A. Jiang, Z. Liu, H. Jin, B. Q. Mercado, M. M. Olmstead, A. L. Balch, *Angew. Chemie – Int. Ed.* **2010**, *49*, 886.
[70] B.-H. Chen, J.-P. Huang, L. Y. Wang, J. Shiea, T.-L. Chen, L. Y. Chiang, *Synth. Commun.* **1998**, *28*, 3515.
[71] A. Domínguez, A. Fernández, N. Gonzalez, E. Iglesias, L. Montenegro, *J. Chem. Educ.* **1997**, *74*, 1227.
[72] F. Ysambertt, F. Vejar, J. Paredes, J. L. Salager, *Colloids Surf., A* **1998**, *137*, 189.

[73] J. N. Israelachvili, *Intermolecular and Surface Forces*, Elsevier Science, Amsterdam, The Netherlands **2011**.
[74] D. I. Kutsarov, I. Rasovic, A. Zachariadis, A. Laskarakis, M. A. Lebedeva, K. Porfyrakis, C. A. Mills, M. J. Beliatis, B. Fisher, K. Bruchlos, S. Ludwigs, S. Logothetidis, S. R. P. Silva, *Adv. Electron. Mater.* **2016**, *2*, 1600362.
[75] A. D. Darwish, P. de Guio, R. Taylor, *Fullerenes Nanotub. Carbon Nanostruct.* **2002**, *10*, 261.
[76] J.-H. Fuhrhop, T. B Wang, *Chem. Rev.* **2004**, *104*, 2901.
[77] B.-C. Wang, H.-W. Wang, H.-C. Tso, T.-L. Chen, Y.-M. Chou, *J. Mol. Struct. THEOCHEM* **2002**, *581*, 177.
[78] I. E. Kareev, I. V. Kuvychko, N. B. Shustova, S. F. Lebedkin, V. P. Bubnov, O. P. Anderson, A. A. Popov, O. V. Boltalina, S. H. Strauss, *Angew. Chemie* **2008**, *120*, 6300.
[79] Z. Drira, V. K. Yadavalli, *J. Mech. Behav. Biomed. Mater.* **2013**, *18*, 20.
[80] N. Hadjichristidis, M. Pitsikalis, H. Iatrou, P. Driva, G. Sakellariou, *Polymers with Star-Related Structures: Synthesis, Properties, and Applications*, Elsevier B.V, Amsterdam, The Netherlands **2012**, Vol. *6*, pp. 29–111.
[81] L. V. Vinogradova, G. A. Polotskaya, A. A. Shevtsova, A. Y. Alent'Ev, *Polym. Sci. Ser. A* **2009**, *51*, 209.
[82] G. Lapienis, *Prog. Polym. Sci.* **2009**, *34*, 852.
[83] X. Qiu, V. Ivasyshyn, L. Qiu, M. Enache, J. Dong, S. Rousseva, G. Portale, M. Stöhr, J. C. Hummelen, R. C. Chiechi, *Nat. Mater.* **2020**, *19*, 330.
[84] N. Welsch, L. Andrew Lyon, *PLoS One* **2017**, *12*, 0181369.
[85] D. J. Hong, E. Lee, M. Lee, *Chem. Commun.* **2007**, 1801.
[86] E. Bakaic, N. M. B. Smeets, M. Badv, M. Dodd, O. Barrigar, E. Siebers, M. Lawlor, H. Sheardown, T. Hoare, *ACS Biomater. Sci. Eng.* **2018**, *4*, 3713.
[87] P. J. M. Stals, J. F. Haveman, R. Martín-Rapún, C. F. C. Fitié, A. R. A. Palmans, E. W. Meijer, *J. Mater. Chem.* **2009**, *19*, 124.
[88] F. Zhang, M. W. A. Skoda, R. M. J. Jacobs, S. Zorn, R. A. Martin, C. M. Martin, G. F. Clark, G. Goerigk, F. Schreiber, *J. Phys. Chem. A* **2007**, *111*, 12229.
[89] D. Lombardo, M. A. Kiselev, S. Magazù, P. Calandra, *Adv. Condens. Matter Phys.* **2015**, *2015*, 151683.
[90] C. Cui, Y. Deng, L. Han, *Sci. China Mater.* **2020**, *63*, 686.
[91] Z. Ulker, C. Erkey, *J. Controlled Release* **2014**, *177*, 51.
[92] R. W. Pekala, J. C. Farmer, C. T. Alviso, T. D. Tran, S. T. Mayer, J. M. Miller, B. Dunn, *J. Non-Cryst. Solids* **1998**, *225*, 74.
[93] I. Levental, P. C. Georges, P. A. Janmey, *Soft Matter* **2007**, *3*, 299.
[94] X. Zhang, N. Sheng, L. Wang, Y. Tan, C. Liu, Y. Xia, Z. Nie, K. Sui, *Mater. Horizons* **2019**, *6*, 326.
[95] Y. J. Wang, X. N. Zhang, Y. Song, Y. Zhao, L. Chen, F. Su, L. Li, Z. L. Wu, Q. Zheng, *Chem. Mater.* **2019**, *31*, 1430.
[96] A. C. Anselmo, S. Mitragotri, *Adv. Drug Delivery Rev.* **2017**, *108*, 51.
[97] F. D. Martinez-Garcia, T. Fischer, A. Hayn, C. T. Mierke, J. K. Burgess, M. C. Harmsen, *Gels* **2022**, *8*, 535.
[98] A. Dasgupta, D. Das, *Langmuir* **2019**, *35*, 10704.
[99] M. P. Hendricks, K. Sato, L. C. Palmer, S. I. Stupp, *Acc. Chem. Res.* **2017**, *50*, 2440.
[100] R. J. Macfarlane, *Nano Lett.* **2021**, *21*, 7432.
[101] W. Kratschmer, L. D. Lamb, K. Fostiropoulos, D. R. Huffman, *Nature* **1990**, *347*, 354.
[102] P. Dallas, S. S. Meysami, N. Grobert, K. Porfyrakis, *RSC Adv.* **2016**, *6*, 24912.
[103] M. P. Gasper, D. W. Armstrong, *J. Liq. Chromatogr.* **1995**, *18*, 1047.
[104] M. Tamaddon, R. S. Walton, D. D. Brand, J. T. Czernuszka, *J. Mater. Sci. Mater. Med.* **2013**, *24*, 1153.
[105] M. Tamaddon, M. Burrows, S. A. Ferreira, F. Dazzi, J. F. Apperley, A. Bradshaw, D. D. Brand, J. Czernuszka, E. Gentleman, *Sci. Rep.* **2017**, *7*, 43519.
[106] C. Y. Chui, A. Bonilla-Brunner, J. Seifert, S. Contera, H. Ye, *J. Mech. Behav. Biomed. Mater.* **2019**, *93*, 61.
[107] J. L. Hutter, J. Bechhoefer, *Rev. Sci. Instrum.* **1993**, *64*, 1868.
[108] C. X. Wang, C. Cowen, Z. Zhang, C. R. Thomas, *Chem. Eng. Sci.* **2005**, *60*, 6649.
[109] H. Hertz, *J. für die reine und angewandte Mathematik* **1882**, *1882*, 156.
[110] L. D. Landau, E. M. Lifshitz, *Course of Theoretical Physics*, Pergamon Press, Oxford **1959**, Vol. *7*.
[111] H. J. Butt, B. Cappella, M. Kappl, *Surf. Sci. Rep.* **2005**, *59*, 1.